J. Theoret. Neurobiol. **2**, 101–125 (1983)
Printed in Australia

NEUROMIME AND COMPUTER SIMULATIONS OF SYNAPTIC INTERACTIONS BETWEEN PACEMAKERS. MATHEMATICAL EXPANSIONS OF EXISTING MODELS*

ANDRÉ F. KOHN** and JOSÉ P. SEGUNDO
Brain Research Institute, Departments of Engineering Systems and Anatomy
University of California, Los Angeles
Los Angeles, CA 90024, U.S.A.

(Received June 15, 1982)

Abstract

An electronic neuromime and simple computer programs simulated synaptic effects on pacemaker neurons corroborating and extending earlier work. Previous experiments showed that with regular IPSP trains within certain rate ranges referred to as "paradoxical" (PS), faster arrivals lead to faster postsynaptic discharges and there is discharge locking in the input-to-output rate relations of 1:2, 1:1 and 2:1. The present simulations showed additional positively sloped segments with locking at ratios such as 2:3, 3:2, 5:3, 7:4 between 1:2, 1:1 and 2:1 PS's. There was, in fact, an enormous, perhaps infinite, number of PS's, and conceivably there are no non-PS's at all.

Using irregular pre- and postsynaptic spontaneous discharges, the main PS's (1:2, 1:1, 2:1) were reduced in width and the additional segments disappeared. For presynaptic interval coefficients of variation (CV) up to 0.20, a small PS persisted in the 1:1 region even with postsynaptic CV's up to 0.10. Simulations of high inhibitory rates showed that while jittery IPSP trains with CV up to 0.20 practically silenced the postsynaptic cells, extremely jittery (quasi-Poisson) ones did not.

Discrepancies between the predictions of a mathematical model (Segundo, 1979) for the presynaptic bounds for PS's and experimental data from crayfish SRO had been attributed tentatively to post-tetanic hyperpolarization (PTH). Neuromime simulations with PTH confirmed this, and showed that a better formulation was to use, instead of the natural pacemaker interval, the shorter one during rebound caused by PTH.

Simulations of the postsynaptic pacemaker with recurrent inhibition (RI) in addition to the usual inhibitory input also showed PS's. If a recurrent IPSP occurred on the average every k spikes, if it was elicited in a "pseudo-random" way, i.e., with a probability 1/k after each spike, the PS's were narrower than when they were elicited "deterministically", i.e., one every k^{th} pacemaker impulse.

Simulations with regular trains of EPSP's also suggested an enormous number of "acceleratory" segments with phase-locking, and minute interposed regions of "paradoxical" deceleration, i.e., where the increase in presynaptic rate caused postsynaptic slowing.

*Supported by funds from the Brain Research Institute, UCLA.
**Supported by FAPESP (Grant 76/180) of São Paulo, Brazil.
Present address: Esc. Politécnica, DEE, Universidade de São Paulo, CP 8174, São Paulo, CEP 01000, Brazil.

The "delay function" plots the arrival time of a PSP relative to the last postsynaptic spike, i.e. the "phase" (ϕ), against the interval lengthening, i.e., the delay (δ). For IPSP's this function is approximated well by a straight line $A\phi + B$; according to a mathematical model (Segundo, 1979), the slope A must be between 0 and 2 for a PS to exist. An analytical-graphical approach showed that for $1<A<2$, there is hysteresis when passing between adjacent PS's by changing the presynaptic mean rate: this has been reported in nature. Under these conditions on A, some PS bounds depend on the initial phase while others do not.

1. Introduction

The present communication reports electronic and computer simulations of regular and irregular, inhibitory and excitatory influences on a pacemaker cell. These cells are common in invertebrate and vertebrate nervous systems and their response to synaptic influences has been studied extensively for IPSP's (Kohn *et al.*, 1981; Perkel *et al.*, 1964; Schulman, 1969; Segundo *et al.*, 1976; Vibert *et al.*, 1979), including computer simulations (Moore *et al.*, 1963; Perkel *et al.*, 1964), and briefly for EPSP's (Segundo and Perkel, 1969).

The present simulations probed further into the following points: (*i*) The existence of positively sloped and locked segments besides the 1:1, 2:1, 1:2; these segments, where greater steady-state presynaptic rates are associated with greater postsynaptic rates are called "paradoxical" when the synapse is inhibitory. (*ii*) The details of the portions between paradoxical segments, *i.e.*, of the "interposed" segments. (*iii*) The influence of postsynaptic post-tetanic hyperpolarization and of recurrent inhibition on the existence and location of paradoxical segments. (*iv*) The development of hysteresis in going from one to another of adjacent paradoxical segments. (*v*) The dependence of locking patterns on the initial "phase", *i.e.*, on the position of the first IPSP arrival relative to the pacemaker spike train. (*vi*) The effects of pre- and/or post-synaptic interval variability on the positively sloped segments. (*vii*) The delay functions for two IPSP's and its relation to the 2:1 locking.

2. Materials and Methods

The neuromime used is an electronic analog designed to represent a "leaky integrator" model of a pacemaker neuron whose mathematical aspects are discussed by Holden (1976) for example, and that has been used profitably. The circuit is detailed in Appendix 1 and consists essentially of a current source feeding a capacitor C in parallel with a resistor R. The capacitor voltage increases exponentially as charge accumulates and when it reaches a certain threshold value, an output pulse ("action potential") is elicited that resets the capacitor to its initial zero voltage.

The neuromime's time scale was 30 to 50 times faster than that of the neuron in the crayfish stretch receptor organ (SRO) (Kohn *et al.*, 1981), thus allowing comparable observations in shorter times. For example, the spontaneous rate of the postsynaptic pacemaker was around 300/s and the typical rates of the SRO were 4/s to 11/s. The neuromime's pacemaker inherent interpulse interval coefficient of variation (CV) was around 1.77×10^{-3}, and therefore negligible. When a less regular output

discharge was desired, a 0 to 50 Hz bandwidth Gaussian "white" noise was added to the integrator capacitor, the power of the noise determining the level of irregularity.

This pacemaker could be affected by inhibitory or excitatory synaptic input (IPSP's or EPSP's) that mimicked natural ones. The effect of a single IPSP or EPSP (or of bursts) on the pacemaker interval was characterized by the "delay function". The time or "phase" ϕ of PSP arrival after a postsynaptic pulse is plotted on the abscissa against the corresponding lengthening $\delta(\phi)$ of the interspike interval on the ordinate (Perkel *et al.*, 1964; Segundo, 1979). Different delay functions were obtained by varying the values of the components in the circuit and/or the duration of the input pulses to the "synapse". With the components mentioned in Appendix 1 and 40 μs input pulses, the delay functions were close to those in the living preparation (Kohn *et al.*, 1981).

Adaptation to sensory stimuli in crayfish SRO is attributed mainly to post-tetanic hyperpolarization (PTH) produced by a sodium electrogenic pump (Nakajima and Takahashi, 1966; Sokolove and Cooke, 1971). Because of the latter, every action potential is followed by a small hyperpolarization which depolarizes back exponentially to the resting voltage. The higher the firing rate, the less time for individual hyperpolarizations to decay and hence the more hyperpolarized the membrane becomes, thus tending to decrease the firing rate. The negative feedback character of the effect on the discharge is clear from this description. PTH in these cells is also a main cause for postinhibitory rebound — the lower firing rate during an inhibitory presynaptic train causes little PTH, and the average postsynaptic potential is less negative than during a spontaneous condition; hence, when the inhibitory train is removed the postsynaptic cell transiently discharges at a rate compatible with the more depolarized membrane potential and therefore higher. It was hypothesized that PTH would cause significant deviations in the paradoxical phase-locked segments from the no-rebound case analyzed theoretically (Segundo, 1979). Indeed, rebound implies a different "latent" postsynaptic spontaneous rate from that without it, and thus would cause different locking ranges. The rebound is not included in the model, where the postsynaptic cell is assumed to return immediately to its spontaneous period after PSP's are interrupted. To test the hypothesis of such a difference, a circuit to mimic the effect of the electrogenic pump was implemented and introduced in the neuromime (see Appendix 1).

Recurrent inhibition (RI) is not uncommon in nervous systems (e.g., Eccles, 1957; Eckert, 1961; Shepherd, 1979). Two types, referred to as "deterministic" and "pseudo-random", were included in some simulations. In the deterministic type, every kth output pulse (i.e., the kth, $2k$th, etc.) generated one recurrent inhibitory pulse. In the pseudo-random type, every pulse generated one RI pulse with a probability of 1/k, i.e., on the average there was an RI pulse every k pulses. The pseudo-random RI simulates the case of some uncertainty in the firing of the inhibitory cell in response to EPSP's (e.g., because of membrane noise, Stevens, 1972). Jansen *et al.* (1970) pointed out that sometimes the recurrent inhibition in the crayfish SRO is one-to-one (i.e., $k=1$), at other times there is one IPSP every kth impulse, and finally, at other times there is an irregularly patterned RI. These facts

motivated our use of deterministic and pseudo-random RI with different "gains". Appendix 2 explains the device that carried out this function.

Regular input trains were obtained from conventional pulse generators. Irregular trains were obtained from an electronic device that generated a Poisson-like process with nearly exponentially distributed intervals. Lower degrees of irregularity were obtained feeding the Poisson into a digital frequency divider whose outputs were nearly gamma-distributed intervals, as in the crayfish experiments (Kohn *et al.*, 1981).

The input and output mean rates were measured with electronic counters by taking average counts over 10s and 50s, depending on the degrees of irregularity. The values were displayed as mean rate transformation (MRT) graphs with presynaptic (input) rates on the abscissa and postsynaptic (output) rates on the ordinate. For the recurrent inhibition simulations, the MRT displayed on the ordinate the postsynaptic rate with recurrent and external input inhibition simultaneously applied and on the abscissa, the external input inhibition rate.

Simple computer programs were written in Basic for the purpose of studying the effect of initial phase on locking and the existence of other positively sloped locked segments. Phase-locking between input and output in the computer programs or the neuromime were detected by visual inspection.

3. Results

IPSP's — Inhibitory Inputs

The mean rate transformation (MRT) for the neuromime subjected to periodic IPSP's (Fig. 1a) showed a zigzag curve with sharp corners between positively sloped or "paradoxical" segments (PS) with 1:2, 1:1, 2:1 (input:output) rate relations, and negatively sloped "interposed" segments (IS) found previously (Kohn *et al.*, 1981; Perkel *et al.*, 1964; Schulman, 1969; Segundo *et al.*, 1976). The widest PS was the 1:1

Table 1

Experimental and theoretical bounds (in s^{-1}) of paradoxical segments.

	Experimental		*Theoretical*		*Corrected theoretical*
	no PTH	w/PTH*	no PTH	w/PTH	
1:1	182–284	250–305	180–284	191–297	238–310
1:2	113–145	138–153	112–146	118–151	132–158
2:1	321–395	470–525	–	–	–
	Spontaneous rate (s^{-1})				
	298.5	313.0			
	Natural period (ms)				
	3.35	*3.20*			
	Delay function				
	$\delta = 0.61\phi + 0.05$	$\delta = 0.576\phi + 0.04$			

*PTH: post-tetanic hyperpolarization.

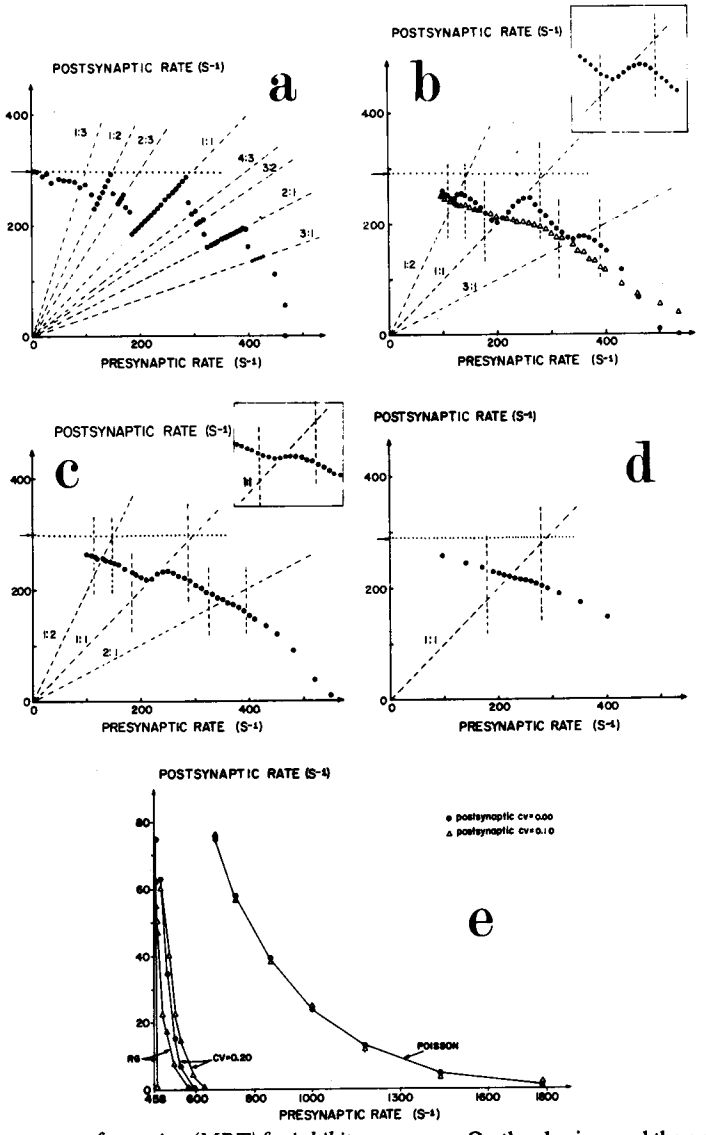

Fig. 1. *Mean rate transformation (MRT) for inhibitory synapse.* On the abscissa and the ordinate, the corresponding pre- and postsynaptic rates over a stationary period. The paradoxical segments are determined with regular trains in each case and their slopes and bounds are indicated by broken lines. The spontaneous postsynaptic rate without IPSP's is indicated by a dotted horizontal line. Different graphs correspond to different pre- or postsynaptic discharge irregularities measured by the interval coefficient of variation (CV). *a. Regular pre- and postsynaptic trains.* Several paradoxical segments are visible. A presynaptic rate above 470/s silenced the postsynaptic firing. *b. Presynaptic interval CV 0.10; Postsynaptic CV 0.03 (circles), 0.10 (asterisks for 1:1 in inset) or 0.35 (triangles). c. Presynaptic CV 0.20; Postsynaptic CV 0.00 (circles) or 0.10 (inset for 1:1 PS). d. Presynaptic CV 0.30. e. High presynaptic rates:* Presynaptic train regular or irregular with CV 0.20 or 1.00 (Poisson); Postsynaptic CV 0.00 (circles) and 0.10 (triangles).

which went, say, from 182 to 284/s occupying a domain of 102/s, followed in order by the 2:1, the 1:2 and the 3:1 (see Table 1). The IS's were very narrow, occupying at most about 20/s in the abscissa scale.

The neuromime showed, in addition, clearcut 2:3, 4:3 and 3:2 PS's: these, though suspected in crayfish, had not been demonstrated (Kohn *et al.*, 1981). Phase-locking between the input and output trains was observed within all PS's.

In different parts of the domain, the postsynaptic mean rate (ordinate in Fig. 1a) showed different sensitivities to presynaptic variations, i.e., the ratios between corresponding changes or the slopes of the graph varied. (*i*) At extreme presynaptic rates, i.e., very low or very high (under 100/s or over 470/s), the postsynaptic rate changed little or not at all in a behaviour that can be referred to as "limiting" or "saturation". (*ii*) Just below the lowest presynaptic rate that stopped the postsynaptic discharge (i.e., 470/s) small presynaptic accelerations produced a precipitous postsynaptic slowing. (*iii*) Within each PS, the postsynaptic rate increased linearly with that of the inhibitory influence and discharges were locked. (*iv*) Within each IS, an overall marked decreasing trend was superimposed upon narrow and alternatively increasing and decreasing portions where locking either occurred only with several pre- and postsynaptic events or was not apparent, respectively. (*v*) Around the junction of a PS with an IS, even small presynaptic changes had marked consequences involving a proportionate slowing and persistent locking on the one side and a greater slowing and complex correlations to the other.

When the input or presynaptic train was irregularized, i.e., when its interval CV increased, while the postsynaptic spontaneous (non-inhibited) discharge remained regular, certain PS's decreased in width and others disappeared. (*i*) When the input CV was 0.10 (Fig. 1b, filled circles), there were PS's only at the 1:2, 1:1 and 2:1 ratios, narrower and with rounded corners at their extremes. (*ii*) When the CV was 0.20 (Fig. 1c, filled circles), only a 1:1 PS interrupted the decreasing trend. (*iii*) When the CV was 0.30 or higher, the mean rate transformation MRT was monotonic decreasing (Fig. 1d). These characteristics agree with those in the crayfish SRO (Kohn *et al.*, 1981).

When the spontaneous postsynaptic train was irregular, PS's also narrowed or disappeared. When, as in the SRO, the spontaneous postsynaptic interval CV was 0.03, a regular presynaptic train caused an MRT with somewhat narrower paradoxical segments, particularly the 3:1 segment that shrunk by a factor of 3 and the 4:3 and 3:2, that disappeared entirely.

When both the pre- and postsynaptic spontaneous discharges were irregularized (an observation not yet performed in living synapses), the PS's were reduced even further (Fig. 1b, inset and triangles; Fig. 1c, inset). For input and spontaneous output CV's equal to 0.10, the 1:2 and 2:1 PS's became almost horizontal and shorter. If then the input CV was increased to 0.20, only a short, almost horizontal PS remained in the 1:1 region; if, finally, the postsynaptic CV became 0.35, no PS's remained (Fig. 1b, open triangles).

Other simulations concentrated on behaviour at high presynaptic rates around where the postsynaptic discharge is suppressed. In the living preparation, it is difficult to obtain sufficient stationary data for the statistical analyses because the post-

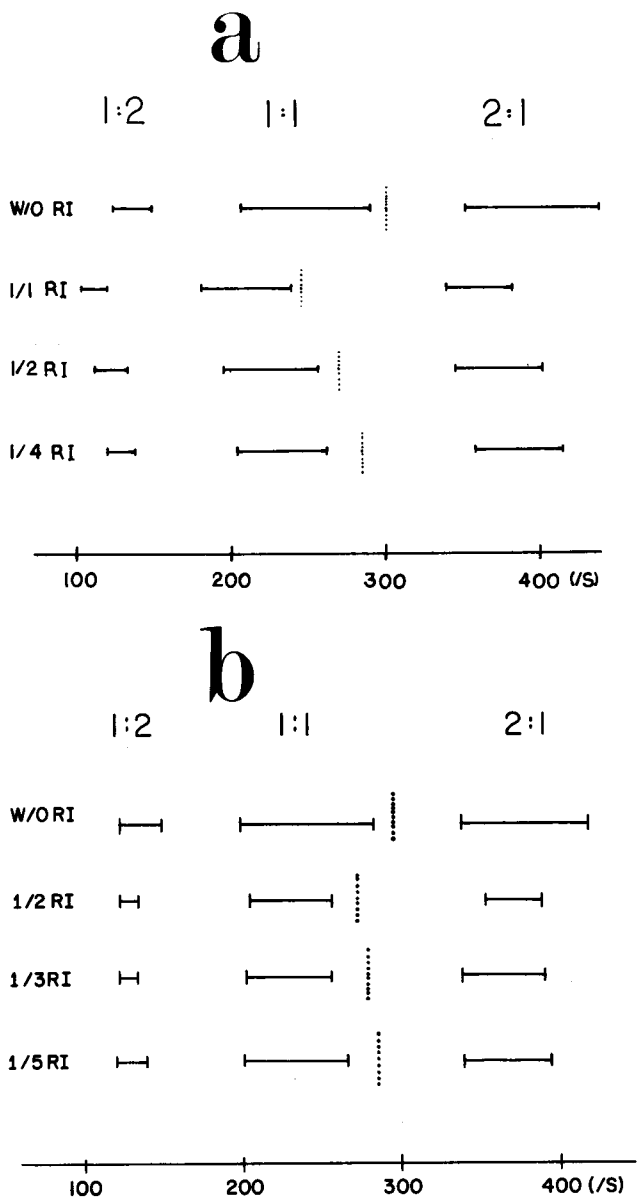

Fig. 2. *Locking ranges for (a) deterministic and (b) pseudo-random recurrent inhibition (RI) for different feedback ratios 1/k.* The horizontal scale is the rate of the regular external presynaptic train. The upper sequence of 3 horizontal bars indicates the ranges where 1:2, 1:1 and 2:1 PS's occurred without RI. The vertical dotted lines are the respective postsynaptic spontaneous rates, higher for no RI than with RI. The spontaneous rates with no RI are different for (a) and (b) because of circuit details.

synaptic neuron tends to escape and start firing (Kohn *et al.*, 1981). When the postsynaptic CV was 0.0, a regular input train that went from 458/s to 466/s (Fig. 1e) caused a very abrupt fall in the postsynaptic rate from 75/s to 0/s, i.e., an average drop of 9.4 postsynaptic impulses/s per each presynaptic increase of 1 impulse per second. For a less regular input (CV = 0.20), the fall in postsynaptic rate was less abrupt: for an input variation of from 470/s to 590/s, it went from about 63/s to 0/s, i.e., an average drop of 2.0/s per presynaptic increase of 1/s. Finally, for a Poisson input, the fall was very slow, resembling an exponential curve, and never reaching zero. If the postsynaptic pacemaker was spontaneously jittery (e.g., with interval CV = 0.10 in Fig. 1e), the fall of the MRT was practically unaltered if the input had a CV = 0.0 or 0.20 or some value in between; the fall was considerably less steep when the input was Poisson.

When post-tetanic hyperpolarization (PTH) was added to the basic neuromime circuit, the MRT for periodic inputs was similar to that in Fig. 1a, except for considerably narrower PS's: the experimental bounds for the 1:1 and 1:2 PS's in Table 1 for a natural postsynaptic interval N = 3.2ms illustrate this, the width of the 1:1 PS, for instance, being 55/s instead of 102/s. The maximum input CV compatible with a PS still was 0.20. A rebound acceleration followed the end of the inhibitory train and was more pronounced the greater the difference between the output inhibited rate and the natural rate. When the input rate was at the lower or upper ends of the 1:1 PS, i.e., at 250/s or 303/s, the first rebound output interval N′ was 2.6ms or 3.1ms, respectively, or when near the ends of the 1:2 PS, at 140/s or 150/s, N′ was 2.9ms or 3.1ms, respectively. Essentially the same results occurred with simulations of inhibitory "synapses" with higher (e.g., 0.83) or lower (e.g., 0.28) slopes in the delay functions.

The postsynaptic pacemaker, when subjected to recurrent inhibition RI of the deterministic type, i.e., with a fed-back IPSP every *k*th postsynaptic impulse, fired with a consistent pattern with a repeating sequence of "long-short interval" if k = 2, or "long-short-short-short" if k = 4. The output pattern was regular if k = 1: in this case, when the phase η of the RI pulse increased, the pacemaker rate decreased almost linearly (as reported by Vibert *et al.*, 1979) with the equation $-21\eta + 277$, where η is measured in ms. The spontaneous rate without RI was 297 impulses/s. The relation between the rates of the independent inhibitory terminal and the inhibited cell, i.e., the usual MRT, for pacemakers inhibited recurrently showed the usual PS (e.g., 1:1, 2:1, 1:2, etc.). For easier viewing, Figure 2a does not show the ordinate axes of the MRT's but only the presynaptic rate ranges where a PS occurred for the RI 1/k ratios 0, 1/1, 1/2 and 1/4. The spontaneous rates (dotted lines in the figure), as well as the PS widths, decreased when RI was present. PS's were observed also with the pseudo-random RI, i.e., when the probability of a recurrent IPSP was 1/k per pacemaker impulse. Here also the widths decreased when compared to the non-RI situation (Fig. 2b). The deterministic and the pseudo-random RI differed in that for the latter the lower bounds of the PS's were never smaller than those without RI (Fig. 2b). The general behaviour of the MRT curves for the non-recurrently inhibited pacemaker subjected to jittery inhibitory inputs was reproduced when RI was present.

Delay functions for a single IPSP were practically linear (correlation coefficients over 0.9). All results presented refer to the delay function $\delta = 0.61\,\phi + 0.049$ (δ and ϕ normalized with respect to the spontaneous period N) unless otherwise indicated. The delay function derived analytically for the leaky integrator with IPSP sizes equal to a times the capacitor voltage at the time of its arrival (as approximately implemented in the neuromime) is:

$$\Delta = \Phi + \zeta\, ln\, [(\exp(-\Phi/\zeta))(1-a)+a]$$

where Δ and Φ are the non-normalized delay and phase, respectively and ζ is the model's time constant RC. It was found experimentally that plots of this function for each of several values of a (e.g., 0.4, 0.6) are good approximations to straight lines.

The normalized delay function for 4 IPSP's at 1000/s was $\delta = 0.98\phi + 0.737$, when the natural period of the pacemaker was 3.50ms. When the input consisted of short high-rate and regular bursts rather than individual pulses, the MRT also showed paradoxical segments and phase-locking. The corresponding 1:1 paradoxical segment (where there was one burst of 4 IPSP's for each postsynaptic AP) was between the input rates of 106/s and 162/s; the 1:2 PS was from 78/s to 101/s.

An experimental-theoretical study was performed to clarify certain aspects of the 2:1 locking, a situation difficult to model, as Segundo (1979) and Kohn (1980) pointed out, because of the dependence of the delay function on the interval between the input IPSP's. Three delay functions were obtained for pairs of IPSP's. Each corresponded to a pair with a different interval I (2.7, 2.8 or 3.0 ms), chosen so that their 1/I rates (i.e., 370.4, 357.1 or 333.3/s, respectively) were within the experimentally determined 2:1 PS (313/s to 389/s). With a postsynaptic spontaneous or natural period of 3.45ms, the results were the delay functions of Table 2. The phase ϕ is measured from the last postsynaptic pulse to the first pulse of the input pair, and the delay is, as usual, the lengthening of the postsynaptic interval. The maximum phase ϕ_m is that which still allows 2 IPSP's to fall within a single postsynaptic interval (and is derived in the section on mathematical considerations): hence, the delay functions of Table 2 are defined in the domain $(0, \phi_m)$.

Table 2

Delay functions for two IPSP's separated by interval I.

		Experimental delay functions (normalized by N = 3.45 ms)	*Maximum phase* ϕ_m (ms)*
Interval I between the 2 IPSP's (ms)	2.7	$\delta_2 = 0.84\phi + 0.51$	2.3
	2.8	$\delta_2 = 0.90\phi + 0.51$	1.9
	3.0	$\delta_2 = 0.93\phi + 0.52$	1.4
2:1 Experimental bounds (s^{-1})	313–389		
2:1 Theoretical bounds (s^{-1})	317–384		

*maximum phase possible.

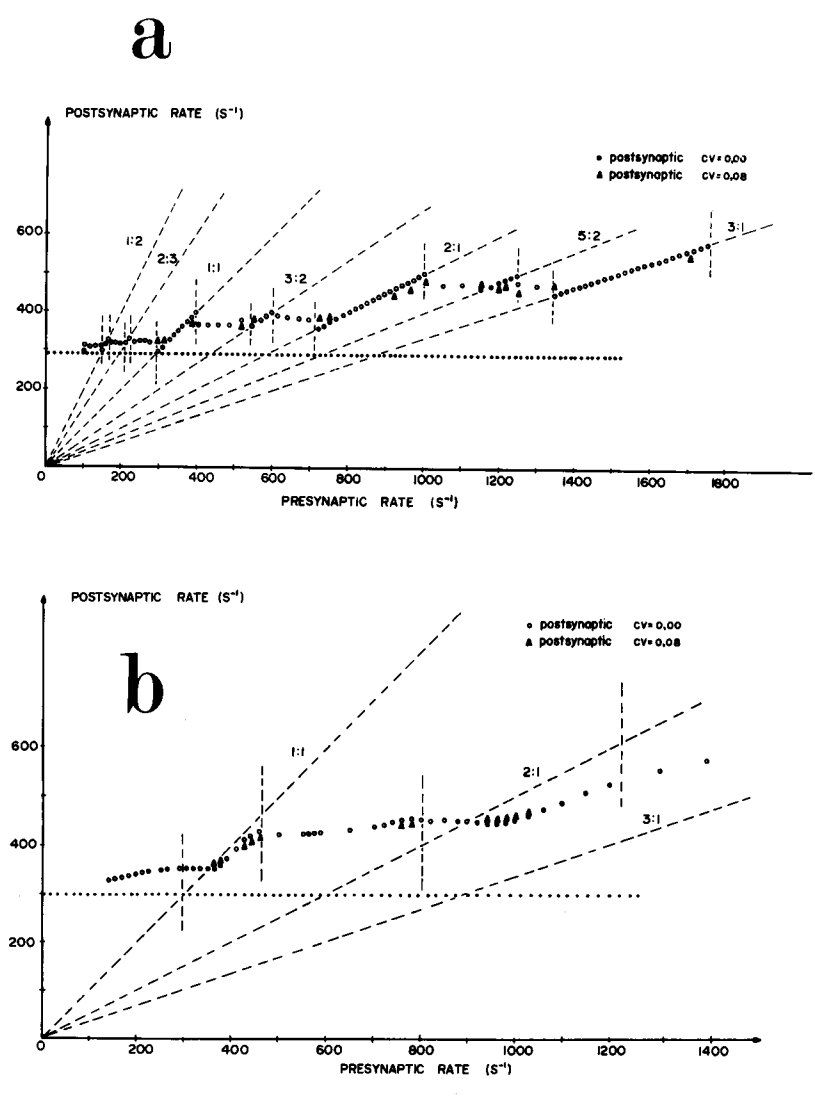

Fig. 3. *Mean rate transformation for excitatory synapse.* Postsynaptic CV 0.00 (circles) or 0.08 (triangles). *a. Regular presynaptic train* (CV = 0.00). The delay function had a "V" shape, with the break point at $\lambda = 0.75$. *b. Jittery presynaptic train (CV 0.20).* The MRT is practically monotonic increasing; the delay function was "V" shaped with $\lambda = 0.64$.

As the interval I between the IPSP's increased, the delay function slope increased somewhat (from 2.7 to 3.0) while the ordinate intercept remained constant; ϕ_m decreased appreciably (e.g., from 2.3 to 1.4). The delay function for 1 IPSP in these simulations was $\delta = 0.55\phi + 0.075$.

A simple program in Basic was developed to allow more precise conclusions about locking ratios and effects of initial phase (also see item *i* in Considerations Regarding

Two Mathematical Models). With the delay function $\delta = 0.6\phi$ (that differed from those in the neuromime only because its intercept was 0 instead of, say, .075) the MRT showed the PS's in Fig. 1a and, in addition, others not discernible there (or nonexistent due to internal noise) and in the ratios of 3:4, 4:5, 5:6, 5:3, 7:4, 9:5. The only consequence of changing the phase of the first or "initial" IPSP was increasing or decreasing the transient time until locking was achieved.

EPSP's — Excitatory Inputs

The mean rate transformation (MRT) for the neuromime subjected to periodic EPSP's showed an increasing trend with positively sloped segments with phase-locking, interrupted by abrupt decreases (Fig. 3a, circles). No output rate was below the spontaneous value. There were clear phase-locked segments at input: output ratios of 1:2, 2:3, 1:1, 3:2, 2:1, 5:2, 3:1, etc. The 3:1 segment (from 1345/s to 1755/s input rates) was broader than the 2:1 (715/s to 1000/s) and this in turn broader than the 1:1 (295/s to 395/s). "Paradoxical" segments (PS) for EPSP regular inputs are those of negative slope; these are the abrupt downward jumps in Fig. 3a (circles). Jumps were smoothed out when the postsynaptic pacemaker had a small intrinsic jitter (interval CV 0.08) (Fig. 3a, crosses), mimicking living pacemaker cells. This small postsynaptic jitter also caused a decrease in the width of the segments and some (e.g., the 1:2, 2:3, 3:2) practically disappeared. When the excitatory input train was irregular, with interval CV 0.20 or larger, the PS's disappeared and the whole MRT (Fig. 3b, CV = 0.20) became monotonic with steep positive slopes within the 1:1 and 2:1 ranges, and a plateau-like region in between.

The delay functions, involving advances or negative delays, resulted in approximately "V" shaped graphs, decreasing steadily from the origin up to a point λ; after λ every EPSP caused a postsynaptic impulse, i.e., the positively sloped branch of the "V" had a unitary slope reaching zero delay for a normalized ϕ equal to 1. λ was 0.75 for Fig. 3a and 0.64 for Fig. 3b.

A mathematical model (Segundo and Kohn, 1981) of the influence of regular EPSP trains upon a postsynaptic pacemaker made the following basic assumptions: (*i*) an

Table 3

Locking ranges of EPSP rate for a pacemaker with period N = 1, synapse with $\lambda = 0.6$. Computer simulations.

locking ratios	*bounds*	*width*
1:3	0.333–0.385	0.520
2:5	0.422–0.448	0.260
1:2	0.500–0.625	0.125
2:3	0.730–0.813	0.830
1:1	1.000–1.667	0.667
3:2	2.083–2.326	0.243
2:1	2.674–4.000	1.326
7:3	4.115–4.274	0.159
5:2	4.310–4.739	0.429
3:1	5.025–6.993	1.968

EPSP causes a shortening of the postsynaptic interval within which it falls with subsequent periods being unaffected; (*ii*) the delay function has a "V" shape, the first branch (from phase 0 to λ) with a slope of $(\lambda - N)/N$, and the second (from phase λ to 1) with a slope of 1. These requirements were satisfied by the neuromime embodiment, and the model's predictions for the locking bounds agreed well with the experimental ones (Fig. 3a, 1:1, 1:2 segments).

A computer program in Basic simulated the interaction of periodic EPSP's with a pacemaker for several values of λ. Phase-locking was observed for all input rates. Table 3 shows for $\lambda = 0.6$ some of the locking ratios and their respective EPSP rate bounds; other locking ratios were found, e.g., 7:18, 11:19, 5:8, 7:11, 7:10, 13:5, 9:4. The initial phase was influential only in determining the speed of convergence towards the locked situation. The same general results were obtained for $\lambda < 0.5$ (see Discussion).

4. Discussion

General

The neuromime and computer simulations suggested that an enormous, perhaps infinite, number of acceleratory and phase-locked segments exist in the steady-state relations between the average intensity of synaptically connected pacemaker cells. Increasing pre- or postsynaptic interval variability, or "jitter", gradually disrupted these segments, with the 2:1 and then the 1:1 disappearing last. The existence of "paradoxical" acceleratory (deceleratory) segments for IPSP's (EPSP's) occurred for presynaptic irregularities with interval CV's up to 0.20. This was true in a variety of situations, i.e., with or without post-tetanic hyperpolarization or recurrent inhibition, and for different synaptic efficacies (as measured by the slope in the delay function).

Simulations cannot give a complete description of the behaviour of a system, as they analyze only a subset of all possibilities. Mathematical analyses, however, provide more generality, and it is likely that a fairly large class of models (to which the leaky integrator belongs) will show paradoxical segments for input train CV's up to 0.20. Therefore, it would be worthwhile to derive analytically the behaviour of a leaky integrator or some more general model subjected to inputs of different CV: this seems a formidable task, however, as even the analytical treatment of the simpler case of exponentially distributed input intervals is complicated (e.g., Cope and Tuckwell, 1979).

IPSP's

The simulations resembled the biological data (Kohn *et al.*, 1981) by showing the zigzag MRT with locked paradoxical segment PS's alternating with interposed ones for presynaptic interval CV's up to 0.20. The neuromime showed similar findings when both the pre- and postsynaptic pacemakers were spontaneously jittery (CV's up to 0.10). Since this kind of variability is not rare in nature, this suggests that a large

number of cells will show locking and paradoxical acceleratory effects. Even though the neuromime and computer embodiments showed for regular inputs a large number of PS's, even a small postsynaptic variability equal to that in crayfish SRO (CV 0.03) was sufficient to reduce or wipe out the secondary PS's, which therefore probably are infrequent in nature.

The general agreement of results with the neuromime and the crayfish SRO implies that the simple leaky integrator pacemaker (a lumped parameter model) with its short-span memory and provided with a simple synaptic input is a sufficient representation of the mechanisms that account for the MRT and phase-locking across that inhibitory synapse: i.e., other dynamic factors like post-tetanic hyperpolarization, refractory periods, dendrosomatic propagation, trigger zone characteristics, do not alter the general qualitative aspects of its performance.

The behaviour at high inhibitory rates indicated that if a presynaptic cell is moderately jittery (e.g., CV 0.20) it can effectively stop the postsynaptic cell for a "long time", but will not if very jittery (e.g., approximately Poisson) (Fig. 1e). Obviously there are other influential parameters not considered in the simulations, like complex synaptic dynamics involving neurotransmitter depletion from the available pool. A less obvious way of stopping a pacemaker, and probably one less likely to occur in nature due to its stringent requirements, is through an adequately effective single PSP or burst of PSP's that occur at an appropriate phase. Such specially weighted and timed PSP's would drive the postsynaptic neuron away from its pacemaker mode towards a non-discharging condition: i.e., it would drive the system away from oscillations in a limit cycle towards rest in the attraction basin of the asymptotically stable equilibrium state (Best, 1979; Guttman *et al.*, 1980; Winfree, 1980).

Recurrent inhibition is an important part of motoneuron circuitry, and it is conceivable that in certain states (e.g., during locomotion) a recurrently inhibited pacemaker neuron receives an almost periodic synaptic influence: hence the interest of the study of paradoxical segments and locking under RI. The practically linear relation between output mean rate and the RI phase in the neuromime mimics well that observed in the crayfish SRO preparation (Vibert *et al.*, 1979). However, when a similar recurrent inhibition experiment is done with the heart-efferent vagal system, at some phase values of the RI a pronounced sinus arrhythmia ensues (Levy, 1978). The RI simulations showed also that pacemakers with less regular discharges, e.g., of a long-short type (deterministic RI with $k = 2$) or more random type (pseudorandom RI) also present paradoxical accelerations and locking with respect to an inhibitory presynaptic pacemaker. This result makes sense if we think of the postsynaptic recurrently inhibited cell as a jittery pacemaker having a low interval CV, e.g., below 0.10 or 0.20 (see Results). The PS's result narrower for the pseudorandom RI because it yields a more jittery equivalent pacemaker than the deterministic RI. Summarizing, RI caused only quantitative changes in the general behaviour of the synaptic interactions; it must be kept in mind, however, that different types of RI can lead as well to marked qualitative changes (Tuckwell, 1978).

EPSP's

These comments on PS's and locking of pacemakers subjected to periodic EPSP's will refer mainly to the simulation results as they relate to a mathematical model (Segundo and Kohn, 1981) since experimental data from living preparations are lacking. The basic postulates of the mathematical model were satisfied by the neuromime and computer embodiments, and the simulations reproduced well its predictions for input rates up the 2:1 PS. For example, the mathematical model predicts 1:2 and 1:1 bounds of 149–170/s and 298–397/s, respectively, for $\lambda = 0.75$. The formulas for 1:r+1 locking are: $((r+1)N)^{-1} < f_E < (rN+\lambda)^{-1}$ where f_E is the presynaptic rate. The 2:1 PS and others at higher rates are difficult to treat analytically and simulations provided new results. The MRT of Fig. 3a (circles) suggests that the widths of PS's of the s:1 type (e.g., 2:1, 3:1, etc.) increase with "s", i.e., when there are more EPSP's per postsynaptic period. There must be some maximum rates, of course, because of the pre- and postsynaptic refractory periods. For more irregular inputs (e.g., CV 0.20 in Fig. 3b), a wide plateau was noted where, from approximately 700 to 1000 input pulses/s, the postsynaptic cell has practically the same rate of about 450/s: i.e., where there is a postsynaptic insensitivity to changes in the presynaptic mean rate.

The "V"-shaped delay functions utilized in the simulations approximate reasonably well the experimental findings in crayfish SRO neurons subjected to pulse depolarizations (except for a smooth transition from one branch to the other of the "V") (Hartline, 1976) and in Aplysia cells with EPSP's (except for delay at small phases) (Segundo and Perkel, 1969). Bursting living cells have delay functions that show delays and advances for a single type of PSP (Pinsker, 1977; Stein, 1974). If the delay functions in our simulations remained nearly linear, but with negative delays (i.e., advances) for small phases and positive delays for large (i.e., $\delta = A\phi + B$ with $B<0$, $A>0$), the mathematical model of Segundo (1979) predicts certain postsynaptic rates below and others above the spontaneous value.

5. Considerations Regarding Two Mathematical Models

(Items *i* to *iv*: Segundo, 1979; item *v*: Segundo & Kohn, 1981)

The diagrams of the spike trains in Fig. 4a provide the following difference equation:

$$\phi_{i+1} = I - N(r+1) + \phi_i - \delta(\phi_i) \tag{1}$$

where I and N are, respectively, the pre- and postsynaptic natural pacemaker periods, r is the number of output pulses per period of the input, $\delta(\phi)$ is the delay function. The delay is positive for IPSP's that lengthen intervals, or negative for EPSP's that shorten them. The new phase (ϕ_{i+1}) versus old phase (ϕ_i) graph is a representation of the equation above, and differs for different delay functions (e.g., Fig. 4b, 5d). The 45° line represents $\phi_{i+1} = \phi_i$; where it is crossed by the $\phi_{i+1} \times \phi_i$ curve there is an equilibrium point or "locking phase" because that phase, once achieved, will

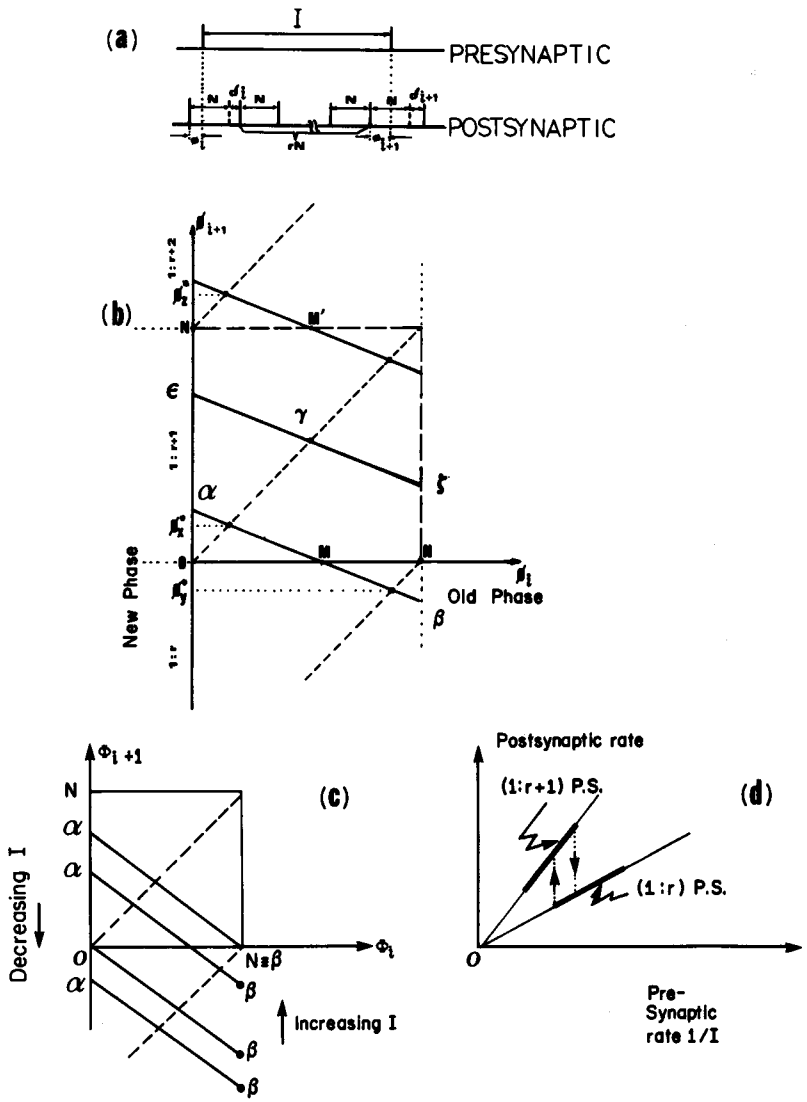

Fig. 4. *Mathematical model for presynaptic pacemaker inhibiting a postsynaptic pacemaker. a. Regular pre- and postsynaptic pacemakers.* The natural periods were I for the former and N for the latter. A presynaptic spike at phase ϕ_i causes a delay $\delta(\phi_i)$. After the perturbed period the postsynaptic pacemaker discharges again with a period N. *b. New phase* ϕ_{i+1}, old phase ϕ_i diagram for a linear delay function $\delta = A\phi + B$ with $1<A<2$. For certain values of the input period I, there are two stable equilibrium phases (e.g., ϕ_x^* and ϕ_y^*). ϕ_x^* is reached if the initial phase $\phi_1<M$, and ϕ_y^* otherwise (see text). *c. Hysteresis.* Starting from the lowest line in the graph with a 1:r locking, increases in I raise the line and when β reaches a point N, 1:r + 1 locking ensues. If thereafter I decreases, the 1:r locking will be achieved again only after the line goes below line 0β. *d. Hysteresis in the MRT.* As the I for the 1:r to 1:r+1 jump occurred for a larger value than the I for 1:r+1 to 1:r, as shown in Fig. *c.*, the hysteresis is revealed in the transition between the two PS's.

perpetuate itself. If the magnitude of the slope of the $\phi_{i+1} \times \phi_i$ curve at an equilibrium point is less than 1, then the equilibrium is asymptotically stable and otherwise it is unstable (Bernussou, 1977); the detailed use of these graphs to analyze locking is illustrated elsewhere (Segundo and Kohn, 1981).

(i) A sufficient condition for hysteresis in a model (Segundo, 1979) is that the slope of the delay function for IPSP's be between 1 and 2.

When the delay function is of the form $\delta(\phi) = A\phi + B$ with $1<A<2$ equation (1) gives us a $\phi_{i+1} \times \phi_i$ curve with a negative slope 1–A, as represented in Fig. 4b by curve $\varepsilon\psi$; two other curves are shown also. The position of each curve depends on the constant term $I - N(r+1) - B$ (obtained from equation (1) by substituting the delay by its expression): hence, variations in the input period I shift the curve vertically. The main quadrant in Fig. 4b corresponds to the 1:r+1 case; a negative new phase ϕ_{i+1} means that the next input pulse occurred before the $(r+1)$th output pulse (see Fig. 4a), which in turn implies a 1:r case, as indicated to the left of Fig. 4b. If the input period I is such that curve $\varepsilon\psi$ is obtained, only one locking phase (point γ in Fig. 4b) is possible in the 1:r+1 rate relation. If the input period is smaller, however, leading to curve $\alpha\beta$, two locking phases would be possible, one ϕ_x^* in the 1:r+1 rate relation and the other ϕ_y^* in the 1:r rate relation. The system will converge to ϕ_x^* and hence, a 1:r+1 locking, if the initial phase is to the left of point M; otherwise, it will converge to ϕ_y^* and hence a 1:r locking.

The possibility of two equilibrium phases thus leads to hysteresis. Indeed, if starting (Figs. 4b,c) at ϕ_y^* with a 1:r locking, the input period I is increased, the line $\alpha\beta$ will be shifted upwards and, when point β surpasses N, a 1:r+1 locking will be installed. If, starting from this 1:r+1 locking, I is decreased, the 1:r+1 relation will be kept until α meets the origin, but as soon as it goes below it, a 1:r locking ensues. This jump happens for a lower I than the one that caused that from 1:r to 1:r+1 (Fig. 4c). Consequently, a clear hysteretical behaviour occurs even with such simple models (Fig. 4d). The required values of A (i.e., between 1 and 2) have been reported, for example, when there are several IPSP's between two successive pacemaker impulses (Kohn *et al.*, 1981). Hysteresis in the region between paradoxical segments was described (Vibert *et al.*, 1981) in the driving of phrenic nerve discharges by forced ventilation in the cat; although in some of those experiments, hysteresis could be due to the mechanism described here since A values were in the range of 0.3–1.4, other complexities of the dynamics involved could be very relevant. Moulopoulos *et al.* (1965) described phase-locking and hysteresis in the dog ventricle subjected to current pulses, but the corresponding delay function is lacking.

To complete the present analysis, the bounds of input periods I and rates $f_I = 1/I$ for which the 1:r+1 locking is independent of the initial phase, and those within which locking depends on the initial phase will be derived. To obtain the former, ϕ_y^* and ϕ_z^* must not exist (Fig. 4b): hence, at $\phi_i = \phi_1 = 0$ (or $\phi_i = \phi_1 = N$) one must have $0<\phi_2<N$, resulting in,

$$[(r+2)N+B]^{-1} < f_I < [(r+A)N+B]^{-1}$$

Between the lower bound of 1:r+1 locking given by this equation and the upper bound of 1:r+2 locking $[(r+1+A)N+B]^{-1}$, there is a range where locking is determined by the initial phase. From Fig. 4b, it can be seen that, if the initial phase is $\phi_1 > M'$, phase-locking is 1:r+1, and otherwise is 1:r+2. M′ can be determined by making $\phi_2 = N$ in the original difference equation (1):

$$M' = [I-(r+2)N-B]/(A-1)$$

So, if the presynaptic rate f_I is between $[(r+1+A)N+B]^{-1}$ and $[(r+2)N+B]^{-1}$, then 1:r+1 locking will ensue if the initial phase ϕ_1 is larger than $(I-(r+2)N-B)/(A-1)$; and 1:r+2 otherwise. These bounds are illustrated in Fig. 5a, where the ordinate is the initial phase and the abscissa the presynaptic rate, with the 1:r+2 and 1:r+1 locking regions indicated by vertical and horizontal shadings, respectively. Fig. 5b shows the computer-simulated discharges of a pacemaker with a period N=1 and delay function $\delta = 1.3\phi$ (i.e., $1<A<2$). The presynaptic discharge has the same period I=2.1 for both pairs of postsynaptic trains and the critical value of M′ is 0.333: in the upper one, the initial phase ϕ_1 is 0.3, and there is 1:2 locking; in the lower one, ϕ_1 is 0.5 and there is a 1:1 locking. This dependence on the initial phase means that if the two pacemakers are locked in a 1:r+1 ratio with an equilibrium phase ϕ_x^*, an extra single impulse from a third neuron that causes a PSP in either pacemaker can shift the phase-locking from 1:r+1 to 1:r+2, and vice versa.

(ii) Delay function with an inverted V shape (Fig. 5c)

This delay function (Fig. 5c) occurs in some crayfish experiments (Kohn *et al.*, 1981, Fig. 8c): *c* is the phase (<N) at which the delay function has a maximum. Using this delay function in the general difference equation (1) gives the new phase-old phase graph in Fig. 5d which again will be displaced upwards if the input period I increases. For the values of I for which the curve intercepts the $\phi_{i+1} = \phi_i$ line, there are two locking phases for 1:r+1 locking, but only one is stable (ϕ_s) because the slope at the other (ϕ_u) is larger than 1. The graph shows also that no matter what the initial phase is (e.g., between *c* and N), there is convergence after some iterations to the stable equilibrium phase. Therefore, to determine the range of input rate f_I where there is 1:r+1 locking, it is necessary to look at the extreme positions of the $\phi_{i+1} \times \phi_i$ curve that still produce a locked phase ϕ_s, i.e., an intersection with the 45° line. The minimum I, where $\phi_{i+1} = \phi_i = 0$, is equal to B+(r+1)N, the maximum, where $\phi_{i+1} = \phi_i = c$, is equal to B+Ac+(r+1)N. In terms of rates (1/I):

$$[(r+1)N+B+Ac]^{-1} < f_I < [B+(r+1)N]^{-1};\ r=0,1,2\ldots$$

These new bounds were used in Kohn *et al.* (1981) to take into account these types of delay functions, and resulted in improved agreement with experimental data from crayfish SRO.

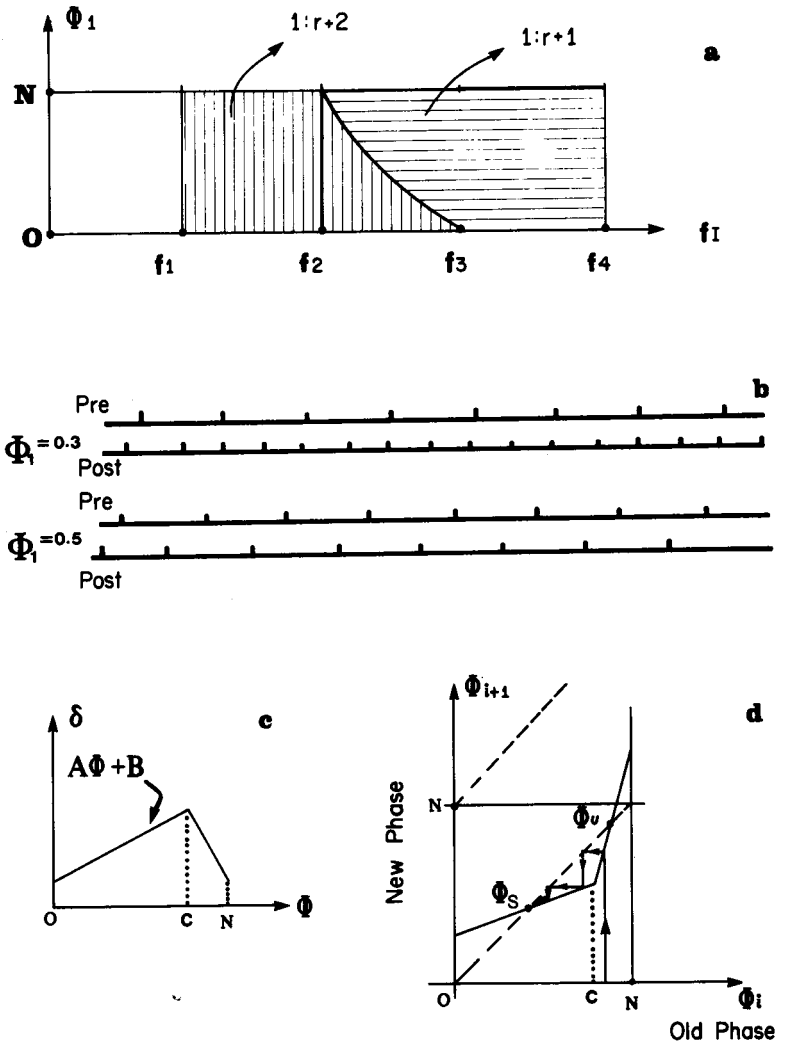

Fig. 5. *Mathematical model for presynaptic pacemaker inhibiting a postsynaptic pacemaker* (cont.). *a. Dependence of locking ratio (for 1<A<2) on the initial phase ϕ_1.* The abscissa and ordinate are the presynaptic rate and the initial phase, respectively. Between f_1 and f_2 there is 1:r+2 locking, between f_2 and f_3, a locking at 1:r+2 for phases ϕ_1 below the dividing line and 1:r+1 above. Between f_3 and f_4, there is 1:r+1 locking. *b. Impulse discharge from a digital computer simulation (A=1.3, I=2.1, N=1.0).* Upper pair is for $\phi_1=0.3$ and leads to 1:2 locking; the lower pair is for $\phi_1=0.50$ and leads to 1:1 locking. *c. Delay function with an inverted "V" shape.* The function increases up to phase *c* and then decreases to the minimum delay for phase N. *d. $\phi_{i+1}\times\phi_i$ diagram for the delay function of item g.* There is one stable equilibrium phase (ϕ_s) to which all trajectories converge, and one unstable equilibrium phase (ϕ_u). $f_1=[(r+3)N+B]^{-1}$, $f_2=[(r+1+A)N+B]^{-1}$, $f_3=[(r+2)N+B]^{-1}$, $f_4=[(r+A)N+B]^{-1}$.

(iii) Post-tetanic hyperpolarization (PTH)

The model's formulas for the ranges of 1:1 and 1:2 locking were in good agreement with the neuromime without PTH (see Table 1); when they were used for simulations with PTH (Table 1), however, marked discrepancies occurred in the lower bounds (24% and 19% for 1:1 and 1:2, respectively). As explained in Methods, PTH causes a rebound interval shortening or rate increase (e.g., Fig. 1 in Kohn *et al.*, 1981). The postsynaptic spontaneous interval that provides better approximations is the rebound one N′ and not the natural one N corresponding to the unstimulated case. N′, measured at the onset of the rebound, brought the theoretical bounds to within 5% of the simulated ones (see Table 1), a considerable improvement over the uncorrected calculations.

(iv) The 2:1 locking

The mathematical model did not predict accurately the bounds of the 2:1 paradoxical segment from the crayfish and neuromime data. An analysis with the neuromime clarified certain issues. Delay functions were evaluated for pairs of IPSP's, each with the particular intervals I 2.7 ms, 2.8 ms, or 3.0 ms, all of which were within the I's in the 2:1 PS and the first and third close to its extremes. Because all three functions showed almost equal A and B values, their average was used for the theoretical predictions. The three functions differed in their domain of definition, i.e., in the maximum phase ϕ_m (Table 2). The three values of ϕ_m suggested an experimental close-to-linear relation to I, but more points would be needed for a strong assertion: hence, instead of using the estimated linear fit, the theoretical relationship between ϕ_m and I was derived. By definition, ϕ_m is the maximum phase ϕ such that $\phi + I = N + \delta$, assuring that the second IPSP of the pair still falls before the next action potential.

Therefore

$$\phi_m + I = \delta_m + N$$

Since $\delta_m = A_1\phi_m + B_1$ where A_1 and B_1 are the parameters for 1 IPSP,

$$\phi_m = \frac{N + B_1}{1 - A_1} - \frac{1}{1 - A_1} \cdot I \tag{2}$$

The relation between ϕ_m and I is indeed linear as suggested in the simulations. Let us define

$$F = \frac{N + B_1}{1 - A_1}, \tag{3}$$

$$E = -\frac{1}{1 - A_1}, \tag{4}$$

so (2) becomes

$$\phi_m = F + IE. \tag{2A}$$

The average delay function for two IPSP's, denoted as $\delta_2 = A_2\phi + B_2$ is found by taking average values of A'_2 and B'_2 from the experimental delay functions (Table 2). Computing the locking phase from (1) and taking into account that for 2:1 locking, two input periods are involved:

$$\phi^* = \frac{2I - N - B_2}{A_2}$$

The locking phase ϕ^*, assuming $0<A_2<1$, will have to be between 0 and ϕ_m for the 2:1 PS, and using (2)

$$0 < \frac{2I - N - B_2}{A_2} < F + IE$$

which, using $f_I = 1/I$ for the input rate, leads to

$$(5) \qquad \frac{2 - A_2 \cdot E}{N + B_2 + A_2 \cdot F} < f_I < \frac{2}{N + B_2}$$

The values of F and E can be computed from (3) and (4) and then substituted into (5), or these equations can be combined resulting in

$$(6) \qquad \frac{2(1 - A_1) + A_2}{(1 - A_1)(N + B_2) + A_2(N + B_1)} < f_I < \frac{2}{N + B_2}$$

To apply (6) to the data in Results, the average delay function for two IPSP's was $\delta_2 = 0.90 \cdot \phi + 0.51$. Therefore, to compute the theoretical 2:1 bounds (Table 2), we use (6) with: $N = 3.45$ ms, $A_1 = 0.55$, $B_1 = 0.075 \times 3.45 = 0.26$ ms, $A_2 = 0.90$, $B_2 = 0.51 \times 3.45 = 1.76$ ms. From Table 2, it is seen that the theoretical bounds are within 1.3% of the experimental values. Had we not taken into account the negative slope dependence of ϕ_m on I (equation 2), and used the original formulation, the lower bound would be in an error of more than 30%. The first step would be to determine experimentally the delay function for one IPSP. The 1:1 PS bounds can be calculated using the model of Segundo (1979), that assumes a linear delay function and $0<A_1<1$, as usually happens in the crayfish SRO (Kohn *et al.*, 1981). Next a presynaptic rate 1/I is chosen that will probably be within the 2:1 region. The criterion used may be to start by taking $1/I = 1.25$ [illegible] the upper bound for the 1:1 PS, then determining experimentally the delay function for two IPSP's separated by that interval I, and with the A'_2 and B'_2, calculating bounds from formula (6). The estimate could be improved by taking three I values within the first approximation of the 2:1 PS, determining experimentally the delay functions for each IPSP pair, and using the average A_2 and B_2 and (6).

A simpler issue is the phase-locking when IPSP's arrive as a succession of equally separated short bursts. As the mathematical model's postulates are satisfied, it is sufficient to determine experimentally a delay function for the burst and with the slope A and intercept B, compute the 1:1 bound. This was checked by the present simulations (see Results) where A was 0.98 and B 0.737 and the 1:1 theoretical bounds (using the formula of item *ii* with $c = 1$) resulted 105/s to 164/s which practically are those found in the simulations.

(v) Use of a mathematical model to predict locking bounds for EPSP inputs

The presynaptic rate bounds for 1:r + 1 locking in a mathematical model (Segundo and Kohn, 1981) are

$$[(r+1)N]^{-1} < f_E < [rN+\lambda]^{-1}$$

λ is the smallest phase at which the EPSP causes an immediate postsynaptic action potential. For $\lambda = 0.6$ the f_E bounds are:

0.3333–0.3846 for the 1:3 locking ratio, 0.5000–0.6250 for the 1:2, and 1.000–1.6666 for the 1:1. These values are practically the same as those found in the simulations with the same λ (see Table 3). There is so far no biological test of this mathematical model.

References

Bernussou, J. (1977). *Point mapping stability.* Pergamon Press, Oxford.

Best, E. N. (1979). Null space in the Hodgkin-Huxley equations: A critical test. *Biophys. J.* **27**, 87–104.

Cope, D. K. and Tuckwell, H. C. (1979). Firing rates of neurons with random excitation and inhibition. *J. Theor. Biol.* **80**, 1–14.

Eccles, J. C. (1957). *The Physiology of Nerve Cells.* Johns Hopkins Press, Baltimore.

Eckert, R. O. (1961). Reflex relationships of the adbominal stretch receptors of the crayfish, I — Feedback inhibition of the receptors. *J. Cell. Comp. Physiol.* **57**, 149–162.

Guttman, R., Lewis, S. and Rinzel, J. (1980). Control of repetitive firing in squid membrane as a model for a neuroneoscillator. *J. Physiol.* **305**, 377–395.

Hartline, D. K. (1976). Simulation of phase-dependent pattern changes to perturbations of regular firing in crayfish stretch receptor. *Brain Res.* **110**, 245–257.

Holden, A. V. (1976). *Models of the Stochastic Activity of Neurones.* Lecture Notes in Biomathematics 12. Springer-Verlag, Berlin.

Jansen, J. K. S., Nja, A., Ormstad, K. and Walloe, L. (1970). Inhibitory control of abdominal stretch receptors of the crayfish. *Acta Physiol. Scand.* **81**, 472–483.

Kohn, A. F. (1980). *Influence of Presynaptic Irregularity on the Inhibition of a Pacemaker in Crayfish and Neuromime.* Thesis, UCLA.

Kohn, A. F., Freitas de Rocha, A. and Segundo, J. P. (1981). Presynaptic irregularity and pacemaker inhibition. *Biol. Cybernetics* **41**, 5–18.

Kuffler, S. W. and Eyzaguirre, C. (1955). Synaptic inhibition in an isolated nerve cell. *J. Gen. Physiol.* **39**, 155–184.

Levy, M. N. (1978). Role of the baroreceptor reflexes in cardiac arrhythmias. *In, Neural Mechanisms in Cardiac Arrhythmias* (Schwartz, P. J. *et al.*, Eds.), pp. 315–322. Raven Press, New York.

Moore, G. P., Perkel, D. H. and Segundo, J. P. (1963). Stability patterns in interneuronal pacemaker regulation. *In, Proc. San Diego Symp. Biomed. Eng.* (Paull, A., Ed.), pp. 184–193. San Diego.

Moulopoulos, S. D., Karkaras, N. and Sideris, D. A. (1965). Stimulus response relationship in dog ventricle *in vivo*. *Am. J. Physiol.* **208**, 154–157.

Nakajima, S. and Takahashi, K. (1966). Post-tetanic hyperpolarization and electrogenic sodium pump in stretch receptor neurone of crayfish. *J. Physiol.* **187**, 105–127.

Ozawa, S. and Tsuda, K. (1973). Membrane permeability changes during inhibitory transmitter action in crayfish stretch receptor cell. *J. Neurophysiol.* **36**, 805–816.

Perkel, D. H., Schulman, J. H., Bullock, T. H., Moore, G. P. and Segundo, J. P. (1964). Pacemaker neurons: effects of regularly spaced synaptic input. *Science* **145**, 61–63.

Pinsker, H. M. (1977). Aplysia bursting neurons as endogenous oscillators. I — Phase response curves for pulsed inhibitory synaptic input. *J. Neurophysiol.* **40**, 527–543.

Schulman, J. H. (1969). *Information Transfer Across an Inhibitor to Pacemaker Synapse at the Crayfish Stretch Receptor.* Thesis, UCLA.

Segundo, J. P. (1979). Pacemaker synaptic interactions: modelled locking and paradoxical features. *Biol. Cybernetics* **35**, 55–62.

Segundo, J. P. and Kohn, A. F. (1981). A model of excitatory synaptic interactions between pacemakers. Its reality, its generality and the principles involved. *Biol. Cybernetics* **40**, 113–126.

Segundo, J. P. and Perkel, D. H. (1969). The nerve cell as an analyzer of spike trains. *In, The Interneuron, UCLA Forum in Medical Sciences* (Brazier, M. A. B., Ed.), pp. 349–389. University of California Press, Los Angeles.

Segundo, J. P., Tolkunov, B. F. and Wolfe, G. E. (1976). Relation between trains of action potentials across an inhibitory synapse. Influence of presynaptic irregularity. *Biol. Cybernetics* **24**, 169–179.

Shepherd, G. M. (1979). *The Synaptic Organization of the Brain.* Oxford, New York.

Sokolove, P. G. and Cooke, I. M. (1971). Inhibition of impulse activity in a sensory neuron by an electrogenic pump. *J. Gen. Physiol.* **57**, 125–163.

Stein, P. G. (1974). Neural control of interappendage phase during locomotion. *Am. Zool.* **14**, 1003–1016.

Stevens, C. F. (1972). Inferences about membrane properties from electrical noise measurements. *Biophys. J.* **12**, 1028–1047.

Tuckwell, H. C. (1978). Recurrent inhibition and afterhyperpolarization: effects on neuronal discharge. *Biol. Cybernetics* **30**, 115–123.

Vibert, J. F., Davis, M. and Segundo, J. P. (1979). Recurrent inhibition: its influence upon transduction and afferent discharges in slowly-adapting stretch receptor organs. *Biol. Cybernetics* **33**, 167–179.

Vibert, J. F., Caille, D. and Segundo, J. P. (1981). Respiratory oscillator entrainment by periodic vagal afferences: an experimental test of a model. *Biol. Cybernetics* **41**, 119–130.

Winfree, A. T. (1980). *The Geometry of Biological Time.* Springer-Verlag, New York.

Appendix 1: The Neuromime Circuit

Fig. A.1 shows the circuit schematic of the neuromime, with functional blocks surrounded by dash-dot lines. The postsynaptic "pacemaker" is represented by the 2μF capacitor which is charged by the 50KΩ trimpot connected to the 5V voltage source. The input of the monostable integrated circuit adds an equivalent resistance R_i in parallel with the 2μF capacitor and hence the time constant RC is given by R_i in parallel with the trimpot times 2μF resulting in about 6 ms for 300/s output spontaneous rate. When the capacitor voltage reaches the threshold (about 2V) of the Schmitt-trigger input of the monostable integrated circuit, the latter fires a pulse of about 30 μs (the "action potential") which resets the capacitor to an initial voltage around 0.6V. After this, as the voltage source is constant, the same exponential growth towards threshold ensues and therefore the same inter-pulse interval will repeat itself, i.e., a periodic or "regular" train is generated. As is common practice in analog and digital simulations, the voltages were scaled to convenient values, e.g., while in a neuron the pacemaker potential could vary from −80mV to −60mV in

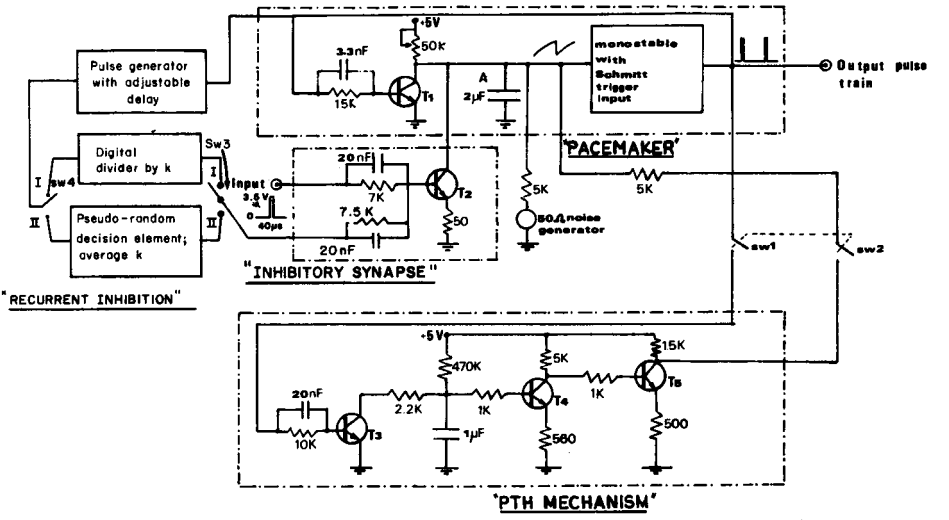

Fig. A.1. *Neuromime circuit diagram.* The postsynaptic pacemaker is of the leaky integrator type and the summation of noise at point A (on the 2μF capacitor) results in intrinsic postsynaptic jitter. Post-tetanic hyperpolarization (PTH) is introduced by closing switches sw1 and sw2. Deterministic recurrent inhibition (RI) is introduced by closing switches sw3 and sw4 to position I and pseudo-random RI to position II.

the neuromime it goes from 0.6V to 2.0V. The inhibitory synapse is implemented by transistor T_2 whose emitter resistor (50Ω) makes the trough of the IPSP less hyperpolarizing when the capacitor voltage is more positive yet keeping the IPSP size larger than that for lower capacitor voltages (i.e., more negative membrane potentials), mimicking natural behaviour. These characteristics also mimic the crayfish SRO inhibitory synapse, where chloride seems to be the main ion involved and the reversal potential is slightly more negative than the resting potential (Ozawa and Tsuda, 1973).

An effect similar to that of an electrogenic pump causing post-tetanic hyperpolarization is introduced by closing switches sw1 and sw2. Every output (i.e., pacemaker) pulse discharges slightly the 1μF capacitor through transistor T_3, transistors T_4 and T_5 providing gain and level adjustment. When the pacemaker rate decreases, the 1μF capacitor is discharged less so its voltage increases, and after being amplified it is summed to the 2μF capacitor of the pacemaker, tending to increase its firing rate (and thus correct for the initial decrease). "Rebound" (Kohn *et al.*, 1981; Kuffler and Eyzaguirre, 1955) occurs in the neuromime because the output rate is low during inhibition and hence the 1μF capacitor has a high voltage. When the stimulus is turned off, the capacitor will slowly decay to its pre-stimulus value that determined the spontaneous rate of the pacemaker. During this time, the higher capacitor (the 1μF one) voltage will cause an overshoot (rebound) in the pacemaker firing rate. The components used for the PTH in Fig. A.1 were optimized for a presynaptic range of 100/s to 310/s.

For simplicity's sake, the feedback or recurrent inhibition (RI) was fed to the same transistor (T_2) that plays the role of "synapse". With switches sw3 and sw4 connected on position I, every *k*th pacemaker pulse will result in an RI pulse applied to T_2. With sw3 and sw4 on position II, the Pseudo-Random Decision Element explained in Appendix 2 gives out an RI pulse for an average of k pacemaker pulses.

An excitatory synapse was simulated in the neuromime by connecting the collector of the PNP transistor T_6 to point A, thus enabling charge to be added to the 2μF capacitor when an input pulse happens at transistor T_7 (Fig. A.2).

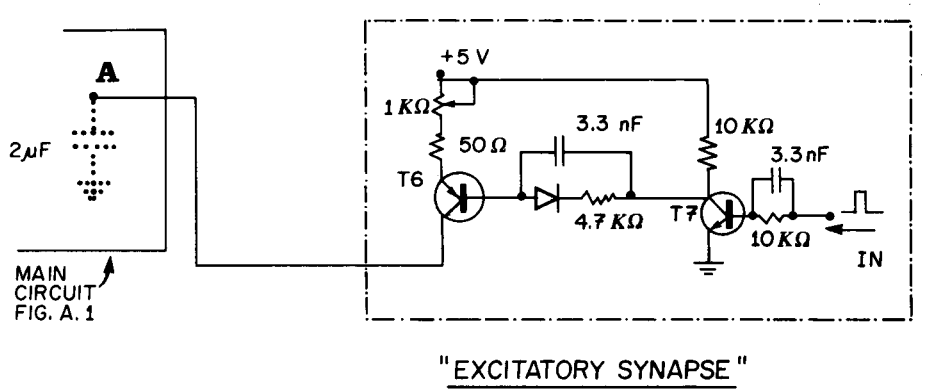

Fig. A.2. *Excitatory presynaptic terminal for inclusion in neuromime.* On the left we show the 2μF capacitor (point A) from the main circuit of Fig. A.1, on the right the "EPSP circuit". The presynaptic "action potential" is applied to the base of T7 through an RC circuit and T6 will add the EPSP to the voltage at point A.

Appendix 2: The Pseudo-Random Decision Element (PRDE)

Figure A.3 shows a simplified block diagram of the PRDE instrument which has at its heart a pseudo-random binary sequence (PRBS) generator composed of a 16-stage shift-register with a convenient exclusive-OR feedback so that only after $2^{16}-1$ input pulses the same number will appear in X. By setting the binary number Y through conveniently pre-programmed switches, the digital magnitude comparator will signal at its output the relationship between the two binary numbers X and Y. Whenever X>Y its output will go to 1 and enable the next input pulse to appear at the output (through the AND gate). For example, if one out of every two input pulses are to be outputted in the average, the switches would be set to 2^{15} and the number X will achieve values above and below 2^{15} in a pseudo-random manner. It is almost as if at each input pulse a Bernoulli experiment takes place to decide if the next output pulse will be gated to the output, or will not.

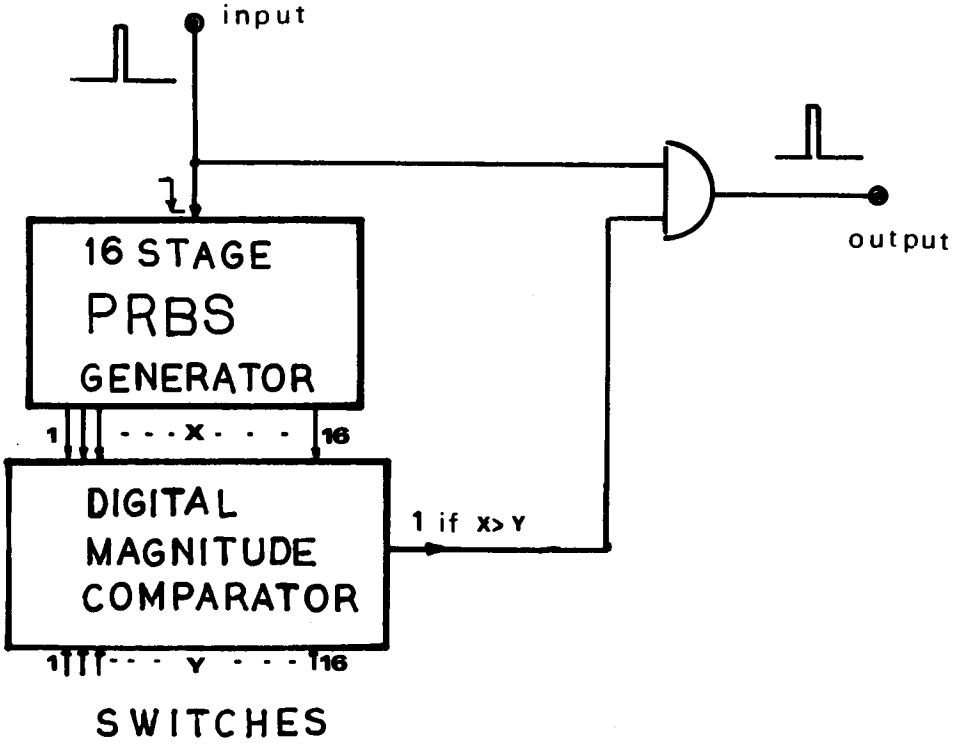

Fig. A.3. *Pseudo-random decision element.* Each input pulse (from the postsynaptic pacemaker) clocks the 16-stage shift register pseudo-random binary sequence (PRBS) generator. The 16-bit word is digitally compared with a word set by switches and if the latter is smaller than the former, the next input is allowed to pass to the output through the AND gate.